

# Behaviour of the Serre Equations in the Presence of Steep Gradients Revisited

J.P.A. Pitt<sup>a,\*</sup>, C. Zoppou<sup>a</sup>, S.G. Roberts<sup>a</sup>

<sup>a</sup>*Mathematical Sciences Institute, Australian National University, Canberra, ACT 0200, Australia*

---

## Abstract

*Keywords:* Serre equations, steep gradients, dam break

---

<sup>1</sup> **1. Introduction**

<sup>2</sup> **2. Serre Equations**

<sup>3</sup> The Serre equations can be derived by integrating the full incompressible Euler  
<sup>4</sup> equations over the water depth, see for example [6]. They can also be derived as an  
<sup>5</sup> asymptotic expansion of the Euler equations, see for example [7]. Assuming a constant  
<sup>6</sup> horizontal bed the one-dimensional Serre equations are [8]

<sup>7</sup> 
$$\frac{\partial h}{\partial t} + \frac{\partial(uh)}{\partial x} = 0 \quad (1a)$$

<sup>8</sup> and

<sup>9</sup> 
$$\underbrace{\frac{\partial(uh)}{\partial t} + \frac{\partial}{\partial x} \left( u^2 h + \frac{gh^2}{2} \right)}_{\text{Shallow Water Wave Equations}} + \underbrace{\frac{\partial}{\partial x} \left( \frac{h^3}{3} \left[ \frac{\partial u}{\partial x} \frac{\partial u}{\partial x} - u \frac{\partial^2 u}{\partial x^2} - \frac{\partial^2 u}{\partial x \partial t} \right] \right)}_{\text{Dispersion Terms}} = 0. \quad (1b)$$

<sup>10</sup>

<sup>11</sup> 
$$\overbrace{\qquad\qquad\qquad\qquad\qquad\qquad}^{\text{Serre Equations}}$$

<sup>12</sup> Where  $u$  is the horizontal velocity over the depth of water  $h$ ,  $g$  is the acceleration due  
<sup>13</sup> to gravity,  $x$  is the horizontal spatial variable and  $t$  is time.

<sup>14</sup> **2.1. Conservation Laws**

<sup>15</sup> The Serre equations are derived from conservation laws for mass ( $h$ ) and momentum ( $uh$ ) [6] thus our numerical methods should conserve these quantities. The total

---

\*Corresponding author

Email addresses: jordan.pitt@anu.edu.au (J.P.A. Pitt),  
christopher.zoppou@anu.edu.au (C. Zoppou), stephen.roberts@anu.edu.au  
(S.G. Roberts)

17 amount of a quantity  $q$  in a system occurring on the interval  $[a, b]$  is measured by

$$18 \quad 19 \quad C_q(t) = \int_a^b q(x, t) dx.$$

20 Conservation of a quantity  $q$  implies that  $C_q(0) = C_q(t) \forall t$  provided the interval is fixed  
21 and the system is closed. Our methods should have this property for the quantities  $h$   
22 and  $uh$ . Additionally the Serre equations admit a Hamiltonian [9, 10]

$$23 \quad 24 \quad \mathcal{H}(x, t) = \frac{1}{2} \left( hu^2 + \frac{h^3}{3} \left( \frac{\partial u}{\partial x} \right)^2 + gh^2 \right) \quad (2)$$

25 which should also be conserved. The Hamiltonian is the sum of the kinetic energies  
26 in the horizontal ( $hu^2$ ) and vertical ( $h^3 (\partial u / \partial x)^2 / 3$ ) directions and the gravitational  
27 potential energy ( $gh^2$ ).

### 28 3. Numerical Methods

29 In Section 5 five different numerical methods are used the first ( $\mathcal{V}_1$ ), second ( $\mathcal{V}_2$ )  
30 and third-order ( $\mathcal{V}_3$ ) methods of [5], the method of El et al. [1] ( $\mathcal{E}$ ) and a second-order  
31 finite difference method ( $\mathcal{G}$ ). These methods all use a fixed grid in time and space, with  
32 subscripts denoting spatial indices and superscripts denoting time indices. Thus for a  
33 quantity  $q$  on our grid  $q_i^n = q(x_i, t^n)$  with the grids uniform such that  $\Delta x = x_i - x_{i-1} \forall i$   
34 and  $\Delta t = t^n - t^{n-1} \forall n$ . A cell is a particularly useful unit of the finite volume method,  
35 the  $i$ th cell is the interval  $[x_i - \Delta x/2, x_i + \Delta x/2]$  centered around  $x_i$ .

36 All methods are stable under the CFL condition [12]. For completeness the two  
37 methods  $\mathcal{G}$  and  $\mathcal{E}$  which are not explicitly published are presented in the Appendix to  
38 allow for replication.

### 39 4. Smoothed Dam Break Problem

40 The discontinuous dam-break problem can be approximated smoothly using the  
41 hyperbolic tangent function. Such an approximation will be called a smoothed dam-  
42 break problem and will be defined as such

$$43 \quad 44 \quad h(x, 0) = h_0 + \frac{h_1 - h_0}{2} \left( 1 + \tanh \left( \frac{x_0 - x}{\alpha} \right) \right), \quad (3a)$$

$$45 \quad u(x, 0) = 0.0m/s. \quad (3b)$$

46 Where  $\alpha$  measures the distance over which 46.117% of the smooth transition between  
47 the two heights of  $h_0$  and  $h_1$  centered around  $x_0$  occurs. Figure 1 demonstrates the  
48 effect of varying  $\alpha$  for the smoothed dam-break problem with  $h_1 = 1.8m$ ,  $h_0 = 1m$  and  
49  $x_0 = 500m$ . These are the same  $h_0$  and  $h_1$  values as those of the dam-breaks presented  
50 by [1] and [2] and will be the values used in Sections 4 and 5.

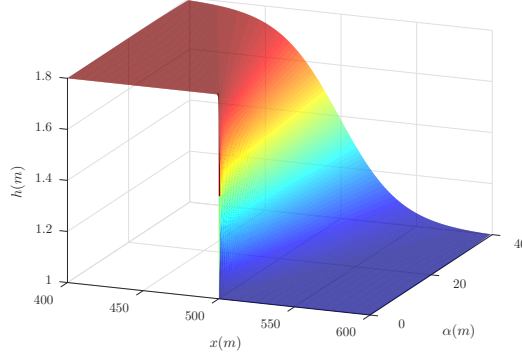


Figure 1: Initial conditions for the smooth dam-break problem with  $h_0 = 1m$ ,  $h_1 = 1.8m$  and  $x_0 = 500m$  as  $\alpha$  varies.

53     *4.1. Measures and Comparisons*

54     There are no analytic results for the Serre equations for either the discontinuous  
 55     dam-break problem or its smoothed approximant. To assess the validity of our results  
 56     we must resort to other comparisons such as measuring the error in the conservation  
 57     of the conserved quantities and measuring the distance between numerical solutions as  
 58      $\Delta x \rightarrow 0$ . Le Métayer et al. [2] and Mitsotakis et al. [3] demonstrated that the analytic  
 59     solution of the shallow water wave equations for the dam-break problem captures the  
 60     mean behaviour of their numerical results. While El et al. [1] derived expressions for  
 61     the leading wave height and speed of an undular bore in the Serre equations. We make  
 62     use of all of these comparisons in Section 5 and so we present some relevant background  
 63     for each here.

64     *4.1.1. Conserved Quantities*

65     The initial conditions of the smoothed dam-break (3) were integrated to get the  
 66     following expressions for  $C_h(0)$ ,  $C_{uh}(0)$  and  $C_{\mathcal{H}}(0)$  provided  $x_0$  is the midpoint of the  
 67     spatial domain  $[a, b]$  in which the smoothed dam-break occurs

68                 
$$C_h(0) = \frac{h_1 + h_0}{2} (b - a),$$

71                 
$$C_{uh}(0) = 0$$

73     and

74                 
$$C_{\mathcal{H}}(0) = \frac{g}{4} \left( h_0^2 - h_1^2 + \alpha (h_1 - h_0)^2 \tanh \left( \frac{a - b}{2\alpha} \right) \right).$$

76     To calculate the total amount of a quantity  $q$  in our numerical solution we fit a  
 77     quartic interpolant of the primitive variables  $h$  and  $u$  over a cell utilising neighbouring  
 78     cells and then apply Gaussian quadrature with 3 points to get the total amount of  $q$  in a

80 cell and then sum this for all cells to get the total amount of  $q$  in our numerical solution  
 81 at time  $t$  which we call  $C_q^*(t)$ . We then measure the error in conservation of a quantity  
 82  $q$  for a numerical method by

$$83 \quad C_1^q = \frac{|C_q(0) - C_q^*(t)|}{|C_q(0)|}. \quad (5)$$

85 Note that for  $uh$  the denominator is 0 and that there is a flux of momentum due to the  
 86 unequal heights at both ends of the domain. To resolve these issues for  $uh$  we measure  
 87 the error in the conservation by

$$88 \quad C_1^{uh} = \left| C_q(0) - C_q^*(t) - \frac{gt}{2} (h(b)^2 - h(a)^2) \right|. \quad (6)$$

90 *4.1.2. Distance between Numerical Results*

91 By measuring the relative distance between results we can assess whether our nu-  
 92 matical solutions are converging as  $\Delta x \rightarrow 0$ . Rather than comparing all numerical  
 93 results to one another we simplify by comparing all our numerical solutions to the one  
 94 with the smallest  $\Delta x$ . For some quantity  $q$  we have a numerical approximation to it  
 95  $q'$  at the locations  $x_i$  and our numerical approximation to it with smallest  $\Delta x$   $q^*$  at the  
 96 locations  $x_j$ . By using grids such that for each  $i$  there is a  $j^*(i)$  such that  $x_i = x_{j^*(i)}$  by  
 97 summing the difference for each  $i$

$$98 \quad L_1^q = \frac{\sum_i |q'_i - q_{j^*(i)}^*|}{\sum_i |q_{j^*(i)}^*|} \quad (7)$$

100 we can measure the relative distance between these numerical solutions on the grid  $x_i$ .

101 *4.1.3. Shallow Water Wave Equation Analytic Solution for the Dam Break*

102 For the discontinuous dam break problem the shallow water wave equations which  
 103 are the Serre equations with dispersive terms neglected can be solved analytically. The  
 104 analytic solution of the shallow water wave equations have been used as a comparative  
 105 tool against numerical results in the literature [2, 3] as they appear to capture the mean  
 106 behaviour of the numerical solutions.

107 An example of the analytic solution of the shallow water wave equations for the  
 108 dam-break problem is presented in Figure 2 at  $t = 30s$ . Region I is the undisturbed  
 109 water upstream of the dam-break at constant height ( $h_1$ ) and velocity (0m/s) and region  
 110 II is the rarefaction fan connecting regions I and III. Regions III and IV are the constant  
 111 height ( $h_2$ ) and constant velocity ( $u_2$ ) state which are separated by  $x_{u_2} = x_0 + u_2 t$  and  
 112 region V is the undisturbed water downstream at constant height ( $h_0$ ) and velocity  
 113 (0m/s) separated from region IV by a shock which travels at velocity  $S_2$ . Expressions  
 114 for the unknown quantities  $h_2$ ,  $u_2$  and  $S_2$  in terms of  $h_0$  and  $h_1$  were given by Wu et al.  
 115 [11]

$$116 \quad h_2 = \frac{h_0}{2} \left( \sqrt{1 + 8 \left( \frac{2h_2}{h_2 - h_0} \frac{\sqrt{gh_1} - \sqrt{gh_2}}{\sqrt{gh_0}} \right)^2} - 1 \right), \quad (8a)$$

118

119  
120

$$u_2 = 2(\sqrt{gh_1} - \sqrt{gh_2}) \quad (8b)$$

121 and

122  
123

$$S_2 = \frac{h_2 u_2}{h_2 - h_0}. \quad (8c)$$

124 From these values the location of the shock separating regions IV and V at time  $t$  is  
 125  $x_{S_2}(t) = x_0 + S_2 t$ . Applying (8) to our dam-break problem heights then  $h_2 = 1.36898m$   
 126 ,  $u_2 = 1.074975 m/s$  and  $S_2 = 3.98835 m/s$  which are demonstrated in Figure 2.

127 **4.1.4. Whitham Modulation for Undular Bores of the Serre Equations**

128 Undular bores for the one dimensional Serre equations were analysed by [1] and an  
 129 expression for the amplitude ( $A^+$ ) and speed ( $S^+$ ) of the leading wave of a bore shown  
 130 in Figure 3 were given

$$131 \quad \frac{\Delta}{(A^+ + 1)^{1/4}} - \left( \frac{3}{4 - \sqrt{A^+ + 1}} \right)^{21/10} \left( \frac{2}{1 + \sqrt{A^+ + 1}} \right)^{2/5} = 0 \quad (9a)$$

133 and

134  
135

$$S^+ = \sqrt{g(A^+ + 1)} \quad (9b)$$

where  $\Delta = h_b/h_0$ , and  $h_b$  is the amplitude of the bore. From this we define  $x_{S^+}(t) = x_0 + S^+ t$  which is the location of the leading wave at time  $t$ . For (9) the height of the bore created by the dam-break is [1]

$$h_b = \frac{1}{4} \left( \sqrt{\frac{h_1}{h_0}} + 1 \right)^2.$$

136 Thus for our dam-break problem heights  $h_b = 1.37082 m$ ,  $\Delta = 1.37082$ ,  $A^+ = 1.73998$   
 137  $m$  and  $S^+ = 4.13148 m/s$ .

138 **5. Numerical Results**

139 We begin by looking into the effect of the initial steepness of the smoothed dam-  
 140 break problem for different  $\alpha$  values by observing what happens as  $\Delta x \rightarrow 0$  and our  
 141 numerical solutions better approximate the true solution of the Serre equations. To  
 142 have the smallest error we use the highest order well validated model  $\mathcal{V}_3$  in the fol-  
 143 lowing investigation. From these results we then investigate numerical results for long  
 144 time scales, how the shallow water wave equations analytic solution and EI's Whitham  
 145 modulation values compare to our results and then finally present some other findings  
 146 about the behaviour of our numerical solutions.

147 All numerical methods used  $\Delta t = 0.01\Delta x$  which is much smaller than required  
 148 by the CFL condition [12] which ensures stability of our schemes or the relation used  
 149 by [1].  $\Delta t$  was chosen to be much smaller than necessary because for a final time of  
 150  $t = 30s$  making  $\Delta t$  small suppresses errors without excessively increasing the runtime  
 151 of the experiments.  $\mathcal{V}_2$  requires an input parameter to its slope limiter and this was  
 152 chosen to be  $\theta = 1.2$  [5].

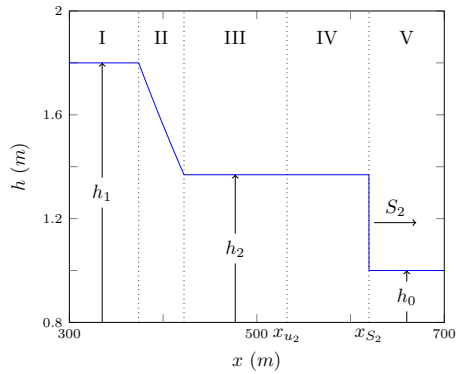


Figure 2: Analytic solution at  $t = 30\text{s}$  of the shallow water wave equations for the dam-break problem with  $h_0 = 1\text{m}$ ,  $h_1 = 1.8\text{m}$  and  $x_0 = 100\text{m}$ .

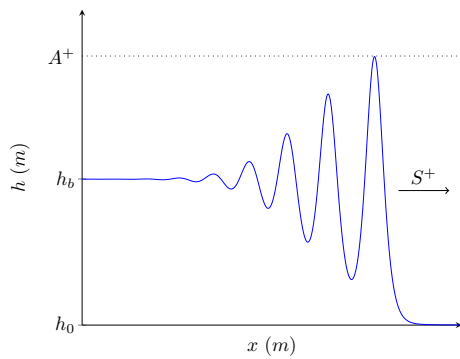


Figure 3: Demonstration of quantities obtained by Whitham modulation for undular bores of the Serre equations.

153    *5.1. Effect of alpha*

154    We observe that there are four types of behaviour as  $\Delta x \rightarrow 0$  depending on the  $\alpha$  and  
155    the numerical method. The four behaviours are identified by the nature of the solutions  
156    around  $x_{u_2}$  when  $\Delta x$  is small and they correspond to different results presented in the  
157    literature. For brevity the only given examples of these behaviours will be the solutions  
158    of  $\mathcal{V}_3$  at  $t = 30s$  on the interval  $x \in [0m, 1000m]$  although they all also occurred for  
159    the numerical results of  $\mathcal{E}$ ,  $\mathcal{G}$  and  $\mathcal{V}_2$  using the same  $\alpha$  and  $\Delta x = 10/2^{10}m$ . All of the  
160    numerical methods presented use dirichlet boundary conditions with  $u = 0m/s$  at both  
161    boundaries and  $h = 1.8m$  on the left and  $h = 1m$  on the right.

162    *5.1.1. Non-oscillatory Behaviour*

163    The first behaviour which will be referred to as the non-oscillatory behaviour has  
164    such smooth initial conditions that no oscillations were introduced by  $t = 30s$  for the  
165    numerical simulations, although given sufficient time the front steepens and an undular  
166    bore will develop. This behaviour is not present in the literature as no authors chose  
167    large enough  $\alpha$ . An example of this behaviour can be seen in Figure 4 for  $\alpha = 40m$   
168    using  $\mathcal{V}_3$  this behaviour was also observed for  $\mathcal{V}_1$ 's numerical solutions. Because this  
169    is a very smooth problem we observe that all numerical results are visually identical for  
170    all  $\Delta x < 10/2^4m$ . We note that  $\mathcal{V}_3$ 's numerical solution has  $h(x_{u_2}) > h_2$  and because no  
171    undulations are present the results of El et al. [1] are not applicable to these solutions.

172    From Table 1 it can be seen that the numerical solutions of  $\mathcal{V}_3$  conserve the con-  
173    served quantities very well for this particular  $\alpha$  for both  $\Delta x$ 's, although the smaller  
174     $\Delta x$ 's numerical results are superior.  $C_1^{uh}$  is the worst performing of the measures be-  
175    cause the smoothed dam-break has such a large transition width that  $h(0m) \neq 1.8m$   
176    and  $h(1000m) \neq 1m$  causing small unquantifiable flows at the boundaries meaning the  
177    system is not closed.

178    These measures verify that we are converging as  $\Delta x \rightarrow 0$  and our solutions are  
179    relatively conservative as the errors for the highest resolution results except for  $C_1^{uh}$   
180    are all at round-off error for each cells value as there are 100,000 cells. Therefore the  
181    numerical result in Figure 4 is an accurate representation of the behaviour of the Serre  
182    equations when  $\alpha$  is sufficiently large and in particular  $\alpha = 40m$ .

183    *5.1.2. Flat Behaviour*

184    The second behaviour will be referred to as the flat behaviour due to the presence  
185    of a constant height around  $x_{u_2}$ , this is the most common behaviour observed in the  
186    literature [2, 3, 4]. This behaviour has oscillations in regions III and IV which are  
187    seperated by a constant height state around  $x_{u_2}$ . An example of the numerical results  
188    for this behaviour can be seen in Figure 5 when  $\alpha = 2m$ , this behaviour was also  
189    observed for  $\mathcal{V}_1$ 's solutions.

190    As  $\Delta x$  decreases the numerical solutions converge so that by  $\Delta x = 10/2^8m$  the  
191    solutions for higher  $\Delta x$  are visually identical. There is also good agreement between  
192    the peak amplitude in region IV ( $A$ ) and  $A^+$  as well as  $h(x_{u_2})$  and  $h_2$ . Although as  
193     $\Delta x$  is decreased in the simulations we observe  $h(x_{u_2}) > h_2$ . Since this method is well  
194    validated for smooth problems and a small  $\Delta x$  has been chosen this suggests that the  
195    mean bore heights in regions III and IV from a dam-break may differ slightly between

$\alpha$ (m)	$\Delta x$ (m)	$C_1^h$	$C_1^{uh}$	$C_1^H$	$L_1^h$	$L_1^u$
40	$10/2^4$	$2.0 \times 10^{-11}$	$1.8 \times 10^{-6}$	$1.2 \times 10^{-8}$	$1.7 \times 10^{-7}$	$2.9 \times 10^{-6}$
40	$10/2^{10}$	$1.8 \times 10^{-11}$	$2.2 \times 10^{-8}$	$3.6 \times 10^{-11}$	$2.5 \times 10^{-11}$	$6.5 \times 10^{-11}$
2	$10/2^4$	$4.9 \times 10^{-14}$	$5.1 \times 10^{-3}$	$8.7 \times 10^{-4}$	$5.0 \times 10^{-3}$	$6.8 \times 10^{-2}$
2	$10/2^{10}$	$4.0 \times 10^{-12}$	$5.0 \times 10^{-9}$	$2.0 \times 10^{-8}$	$1.8 \times 10^{-7}$	$2.3 \times 10^{-6}$
0.4	$10/2^4$	$9 \times 10^{-14}$	$4.8 \times 10^{-3}$	$1.0 \times 10^{-3}$	$6.8 \times 10^{-3} \dagger$	$9.9 \times 10^{-2} \dagger$
0.4	$10/2^{10}$	$3.9 \times 10^{-12}$	$5.0 \times 10^{-9}$	$2.0 \times 10^{-8}$	$3.6 \times 10^{-7} \dagger$	$5.0 \times 10^{-6} \dagger$
0.1	$10/2^4$	$7.6 \times 10^{-14}$	$4.8 \times 10^{-3}$	$1.0 \times 10^{-3}$	$7.0 \times 10^{-3} \dagger$	$1.0 \times 10^{-1} \dagger$
0.1	$10/2^{10}$	$3.9 \times 10^{-12}$	$4.6 \times 10^{-8}$	$7.6 \times 10^{-7}$	$5.0 \times 10^{-7} \dagger$	$6.4 \times 10^{-6} \dagger$

Table 1: All errors in conservation  $C_1^q$  (6) for the conserved quantities and relative distances  $L_1^q$  (7) of the primitive variables for numerical solutions of  $\mathcal{V}_3$ .  $L_1^q$  uses the numerical solution with  $\Delta x = 10/2^{11}m$  as the high resolution basis of comparison and  $\dagger$  indicates where the interval  $[520m, 540m]$  has been omitted from the comparison.

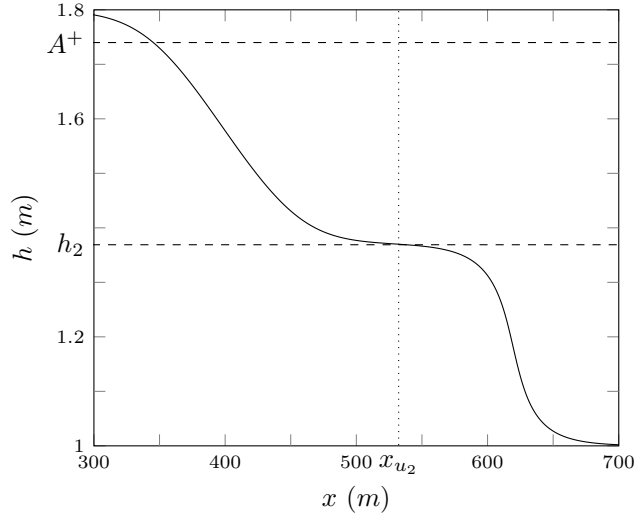


Figure 4: Numerical results of  $\mathcal{V}_3$  at  $t = 30s$  for the smooth dam-break problem with  $\alpha = 40m$  for  $\Delta x = 10/2^4m$  (—).

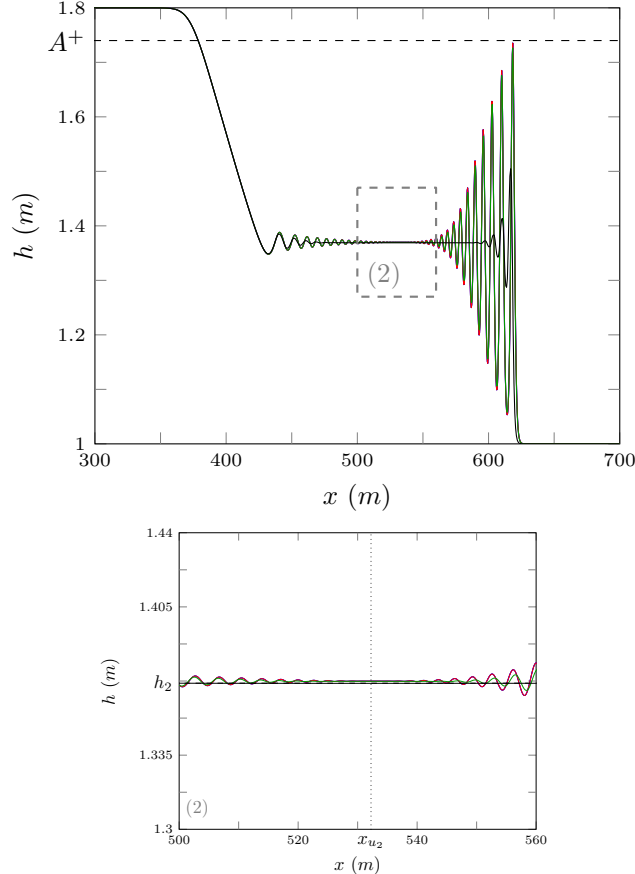


Figure 5: Numerical results of  $\mathcal{V}_3$  at  $t = 30s$  for the smooth dam-break problem with  $\alpha = 2m$  for  $\Delta x = 10/2^{10}m$  (—),  $10/2^8m$  (—),  $10/2^6m$  (—) and  $10/2^4m$  (—).

the shallow water wave equations and the Serre equations. These solutions replicate the behaviour of the results of Mitsotakis et al. [4] who use the same  $\alpha$  but different  $h_0$  and  $h_1$ .

Table 1 demonstrates good conservation of the conserved quantities for our numerical solution with  $\Delta x = 10/2^{10}m$ , although only the errors in conservation of  $h$  are at the size of round-off errors. The  $L_1$  measures demonstrate that our solutions are very close to the numerical solution with  $\Delta x = 10/2^{11}m$ .

These results demonstrate that the numerical solutions in Figure 5 are an accurate representation of the nature of the Serre equations provided  $\alpha$  and  $\Delta x$  are appropriate supporting the numerical solutions of [4] who used the same  $\alpha$  but different  $h_0$  and  $h_1$  values.

#### 5.1.3. Node Behaviour

The third behaviour will be referred to as the node behaviour and it was observed by [1]. The node behaviour's main feature is that the oscillations in region III and IV

210 decay and appear to meet at  $x_{u_2}$  as can be seen in Figure 6 when  $\alpha = 0.4m$ . Unfortunately  
 211 these numerical solutions are not visually identical for the higher resolutions as they  
 212 were in the flat behaviour example. However, the numerical solutions are getting closer  
 213 to one another and convergence is expected for the smaller  $\Delta x$  because the problem is  
 214 still smooth. In these results  $A^+$  is a good estimator for  $A$  and the oscillations in regions  
 215 III and IV appear to be around  $h_2$ . This behaviour was observed by [1] for  $\mathcal{E}$  and  
 216 indeed we have replicated it. This behaviour was not observed in  $\mathcal{V}_1$ 's solutions up to  
 217  $\Delta x = 10/2^{10}m$  with  $\alpha = 0.001m$  as  $\mathcal{V}_1$  introduces diffusive errors that severely dampen  
 218 oscillations. This explains why [2] using  $\mathcal{V}_1$  could not replicate the results of [1]. It  
 219 was found that an  $\alpha$  of at least  $0.4m$  is required to recover the node behaviour this  
 220 explains why Mitsotakis et al. [3] and Mitsotakis et al. [4] using  $\alpha$ 's of  $2m$  and  $1m$   
 221 respectively could not replicate the results of El et al. [1].

222 Figure 6 demonstrates that our numerical solutions have not converged, however  
 223 this is only in the area around  $x_{u_2}$ . This indicates that the behaviour of our solutions  
 224 away from  $x_{u_2}$  are consistent, in particular our results for  $A$ . The larger distance be-  
 225 tween numerical solutions means we cannot get a meaningful measure of  $L_1$  for the  
 226 whole domain. However, by omitting an interval around  $x_{u_2}$  such as  $[520m, 540m]$  a  
 227 meaningful measure of  $L_1$  can be calculated, this modified  $L_1$  is presented in Table 1.  
 228 These modified  $L_1$ 's demonstrate that our solutions are close to one another and have  
 229 converged away from  $x_{u_2}$ , so that increasing the grid resolution further would only  
 230 cause a significant change in the numerical solutions around  $x_{u_2}$ . Table 1 shows that  
 231 for  $\Delta x = 10/2^{10}m$  our conserved quantities are very well conserved by our numerical  
 232 solution.

233 These results suggest that although we have not yet fully converged these numerical  
 234 solutions are close to reasonable solutions of the Serre equations for the smoothed dam-  
 235 break problem for an appropriate  $\alpha$  value supporting the numerical solutions presented  
 236 by El et al. [1].

#### 237 5.1.4. Growth Behaviour

238 The fourth behaviour will be referred to as the growth behaviour due to the oscilla-  
 239 tions in regions III and IV growing around  $x_{u_2}$  as can be seen in Figure 7 for  $\alpha = 0.1m$ .  
 240 This behaviour could not be replicated for  $\mathcal{V}_1$  and has hitherto not been published.

241 Figure 7 shows that the disagreement in the numerical results is concentrated around  
 242  $x_{u_2}$ .  $A$  is again predicted by  $A^+$  well and the oscillations in regions III and IV are around  
 243  $h_2$ . The different resolution numerical results are getting closer to one another, but the  
 244 sudden change in behaviour around  $x_{u_2}$  makes it difficult to assert that large growths  
 245 in amplitude are not possible around  $x_{u_2}$  as we take  $\Delta x$  smaller. However, for nu-  
 246 mercial solutions with  $\alpha = 0.001m$  and  $\Delta x = 10/2^{11}m$  these oscillations around  $x_{u_2}$   
 247 stayed within the interval  $[1.455m, 1.3m]$ . The number of oscillations is the same for  
 248  $\Delta x = 10/2^{10}m$  in Figures 6 and 7 with different  $\alpha$  values so that the change in behaviour  
 249 is a result of the difference in amplitudes of the oscillations and not an increase in their  
 250 number.

251 The interval  $[520m, 540m]$  has been omitted from  $L_1$  in Table 1 due to the lack of  
 252 convergence in this region. The  $L_1$  measures for the numerical solution with  $\alpha = 0.1m$   
 253 and  $\Delta x = 10/2^{10}m$  are very close but slightly larger than those for the node behaviour,  
 254 confirming that our numerical solutions are correctly capturing the behaviour of the

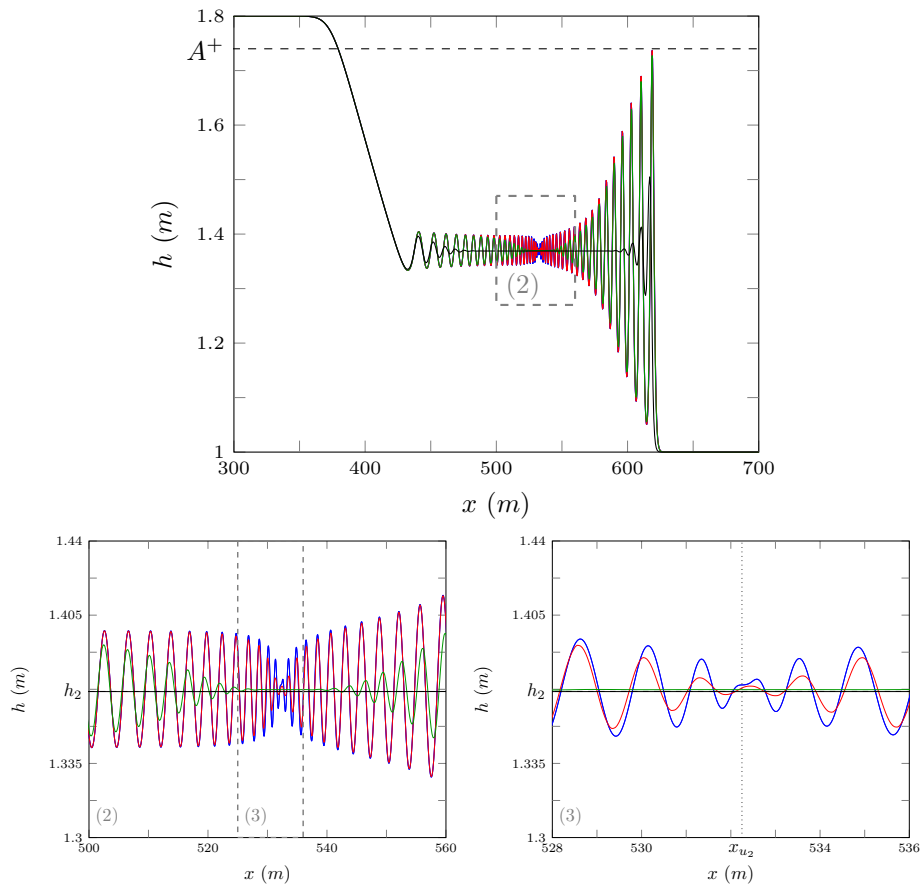


Figure 6: Numerical results of  $\mathcal{V}_3$  at  $t = 30s$  for the smooth dam-break problem with  $\alpha = 0.4m$  for  $\Delta x = 10/2^{10}m$  (—),  $10/2^8m$  (—),  $10/2^6m$  (—) and  $10/2^4m$  (—).

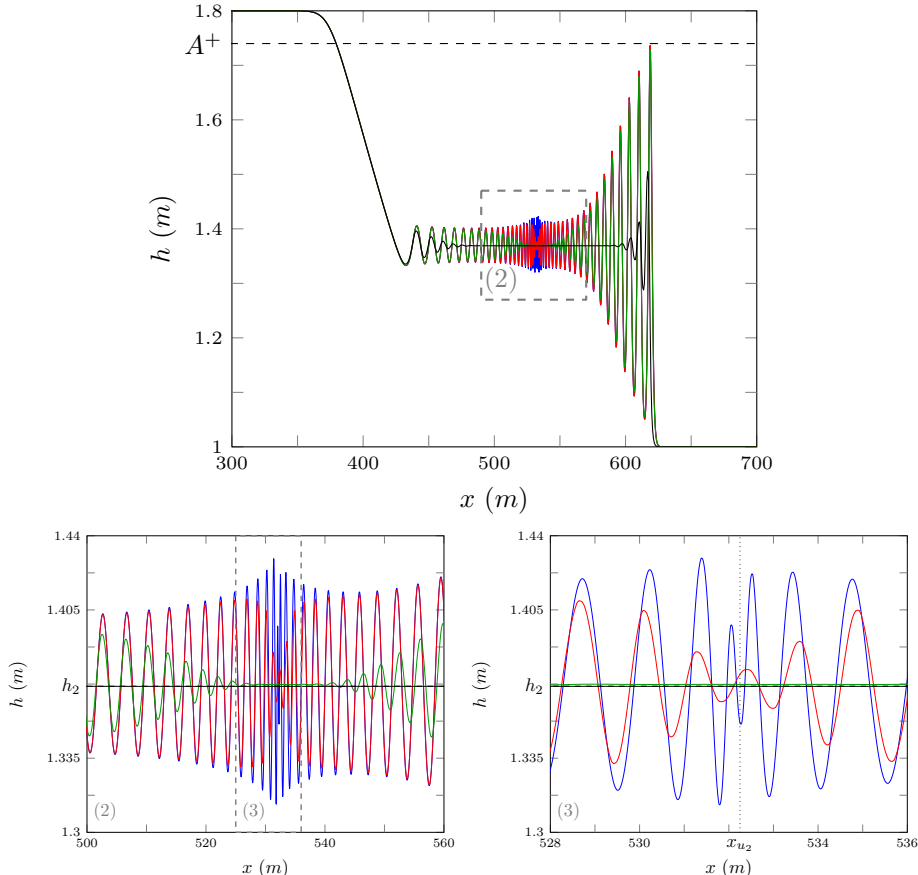


Figure 7: Numerical results of  $\mathcal{V}_3$  at  $t = 30s$  for the smooth dam-break problem with  $\alpha = 0.1m$  for  $\Delta x = 10/2^{10}m$  (—),  $10/2^8m$  (—),  $10/2^6m$  (—) and  $10/2^4m$  (—).

255 Serre equations for this problem away from  $x_{u_2}$ . The errors in conservation are small,  
 256 and in particular our conservation of  $h$  is as good as those in node and flat behaviour.  
 257 The errors in conservation of  $uh$  and  $\mathcal{H}$  however are larger than the previous behaviours  
 258 examples by a factor of 10.

259 Since this our numerical results have poorer convergence and conservation and  
 260 cannot be found in the literature, we resort to using many different methods to support  
 261 the numerical solutions of  $\mathcal{V}_3$ . To remove the possibility that some effect from the  
 262 reformulation of the Serre equations or the elliptic solver of the  $\mathcal{V}_i$  methods are the  
 263 cause we use make use of  $\mathcal{G}$  and  $\mathcal{E}$ .  $\mathcal{G}$ ,  $\mathcal{E}$ ,  $\mathcal{V}_1$  and  $\mathcal{V}_3$  are applied to the same initial  
 264 conditions with the same grid resolutions as above and the results were plotted in Figure  
 265 8.  $\mathcal{V}_2$  has been omitted from this figure for clarity because its solution is very close to  
 266  $\mathcal{V}_3$ .

267 The first observation is that  $\mathcal{V}_1$  has not recovered a growth behaviour. This is be-  
 268 cause  $\mathcal{V}_1$  is very diffusive [5], dampening these oscillations. To resolve such behaviour

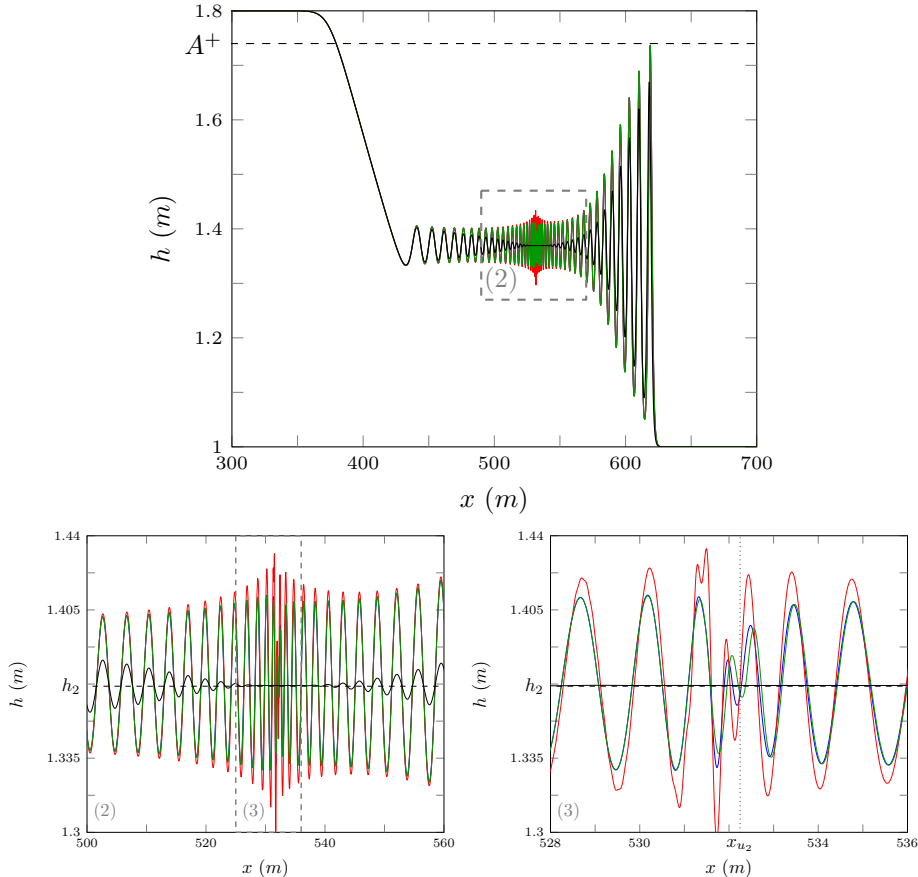


Figure 8: Numerical results for the smooth dam-break problem with  $\alpha = 0.1m$  and  $\Delta x = 10/2^{10}m$  for  $\mathcal{G}$  (—),  $\mathcal{E}$  (—),  $\mathcal{V}_3$  (—) and  $\mathcal{V}_1$  (—).

for  $\mathcal{V}_1$  would require restrictively small  $\Delta x$  and as such this has not been observed in the simulations. Secondly, all high-order methods recover this growth behaviour and disagree only in the region around  $x_{u_2}$ . The absence of the growth behaviour in the findings of El et al. [1] is the result of smoothing of the initial conditions [13].

Generally dispersive methods overestimate the size and number of oscillations of the true solution while diffusive methods underestimate the size and number of oscillations in the true solution. Since  $\mathcal{V}_3$  is diffusive as can be seen in Figure 7 and  $\mathcal{G}$  is dispersive the true analytic solution should exist between  $\mathcal{V}_3$  and  $\mathcal{G}$ . As  $\mathcal{G}$  and  $\mathcal{V}_3$  have the same number of oscillations we expect that the true solution will have the same number of oscillations with different amplitudes.  $\mathcal{G}$  has very similar numerical solutions to  $\mathcal{V}_2$  and  $\mathcal{V}_3$  which are preferred by the authors due to their robustness and superior conservation of quantities.

These results demonstrate that while our numerical results have not converged as  $\Delta x \rightarrow 0$  the agreement of all the discussed methods of sufficiently high order indicates

283 that these results are representative of actual solutions of the smoothed dam-break prob-  
 284 lem with low  $\alpha$  for the Serre equations. This is the same behaviour that we observe for  
 285  $\mathcal{V}_2$  and  $\mathcal{V}_3$  with the same  $\Delta x$  and  $\Delta t$  for the dam-break.

### 286 5.2. Long time

287 To assess long term behaviour a smoothed dam-break was solved by  $\mathcal{V}_3$  with  
 288 the same parameters on a larger domain  $x \in [-900m, 1800m]$  for a longer time  $t \in$   
 289  $[0, 300s]$ . The results of  $\mathcal{V}_3$  with  $\alpha = 0.1m$  and  $\Delta x = 10/2^9 m$  and  $10/2^8 m$  at  $t = 300s$   
 290 are presented in Figure 9. For this problem these parameters result in the growth be-  
 291 haviour, however after sufficient time this growth behaviour has decayed back into a  
 292 flat behaviour although there are still small oscillations present in the middle region.

293 To track the decaying of the oscillations for  $\mathcal{V}_3$ 's solution around  $x_{u_2}$  a snapshot  
 294 of the area around  $x_{u_2}$  has been plotted for different times in Figure 10. It can be seen  
 295 that at  $t = 30s$  the solution exhibits the growth behaviour but as time progresses the  
 296 region around  $x_{u_2}$  has decayed into the node behaviour by  $t = 100s$  and then into the  
 297 flat behaviour observed at  $t = 200s$  and  $t = 300s$ . This is most likely due to the  
 298 accumulation of diffusive errors of the numerical method with Figure 9 demonstrating  
 299 that over this time span we are not close to convergence of the numerical results.

### 300 5.3. Shallow water wave equation comparison

301 The shallow water wave equations have been used as a guide for the mean be-  
 302 haviour of the solution of the Serre equations for the dam-break problem in the litera-  
 303 ture [2, 3]. We assess their applicability by plotting  $h - h_2$  and  $u - u_2$  for the smoothed  
 304 dam-break problem with  $\alpha = 0.1m$  and  $\Delta x = 10/2^9 m$  in Figure 11 for  $t = 30s$  and  
 305 Figure 12 for  $t = 300s$ .

306 From these results it can be seen that over short time spans both  $h_2$  and  $u_2$  are good  
 307 approximations to the mean behaviour of the fluid with both plots oscillating around 0.  
 308 However after sufficient time the mean velocity and height of the bore have diverged  
 309 slightly from the shallow water wave equation values  $h_2$  and  $u_2$ . With  $h_2$  being an  
 310 underestimate and  $u_2$  being an overestimate. While Figure 9 demonstrates that  $S_2$  is a  
 311 worse approximation than  $h_2$  and  $u_2$ .

#### 312 5.3.1. Contact discontinuity

313 The contact discontinuity is the location of the node in the node behaviour [1]  
 314 and the growth of the oscillations in the growth behavior, we have demonstrated that  
 315 this is at about  $x_{u_2}$  as can be seen in Figures 6 and 7. Figures 11 and 12 show a more  
 316 fundamental property of the contact discontinuity, that it is the transition between when  
 317  $h$  and  $u$  are anti-phase to the left and when  $h$  and  $u$  are in-phase to the right.

318 By inspecting the phase velocity for the linearised Serre equations

$$319 \quad v_p = u \pm \sqrt{gh} \sqrt{\frac{3}{h^2 k^2 + 3}} \quad (10)$$

320 with wave number  $k$ , it can be seen that as  $k \rightarrow \infty$  then  $v_p \rightarrow u$  and as  $k \rightarrow 0$   
 321 then  $v_p \rightarrow u \pm \sqrt{gh}$ . Therefore when  $u$  and  $h$  are anti-phase this corresponds to the  
 322 negative branch of the phase velocity  $u - \sqrt{gh} \sqrt{3/(h^2 k^2 + 3)}$  and when  $u$  and  $h$  are

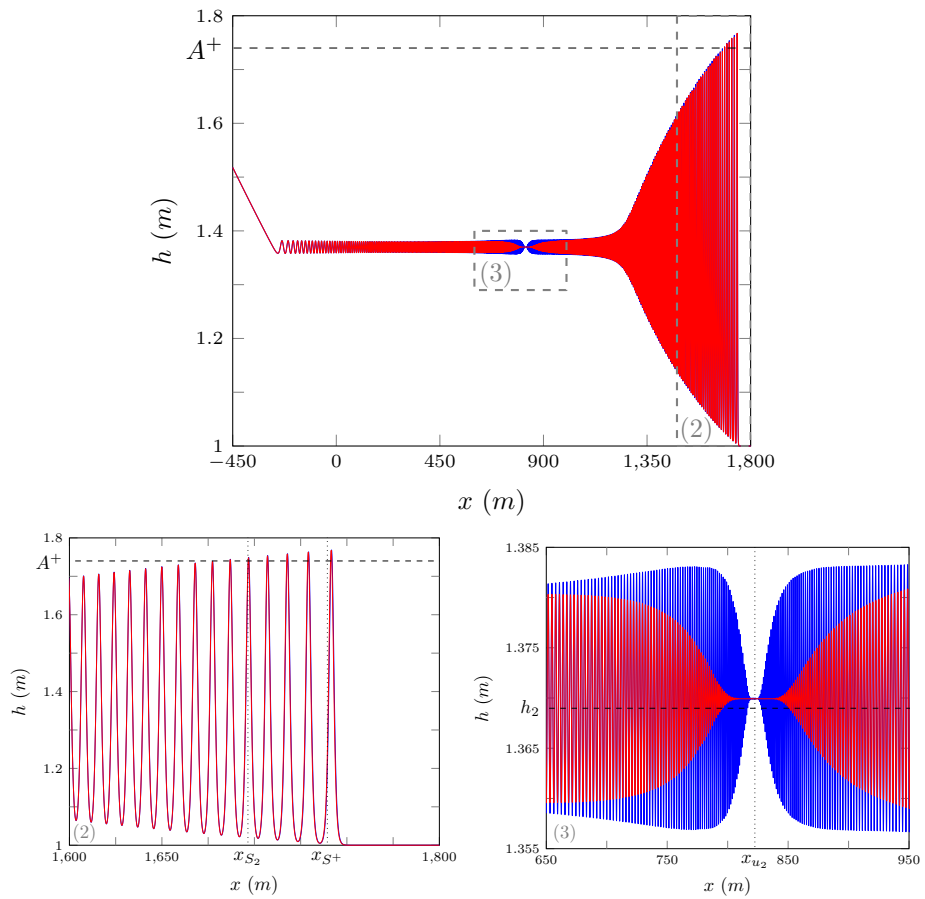


Figure 9: Numerical solution of smooth dam-break problem at  $t = 300s$  by  $\mathcal{V}_3$  with  $\alpha = 0.1m$  for  $\Delta x = 10/2^9 m$  (blue) and  $10/2^8 m$  (red).

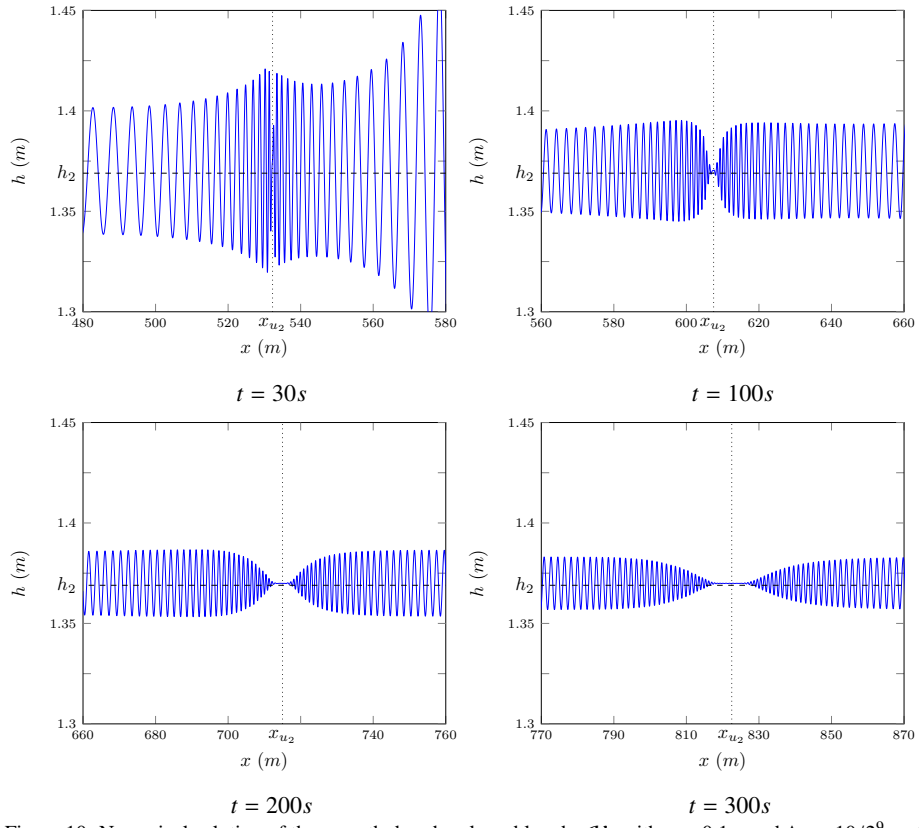


Figure 10: Numerical solution of the smooth dam-break problem by  $\mathcal{V}_3$  with  $\alpha = 0.1m$  and  $\Delta x = 10/2^9 m$  at various times.

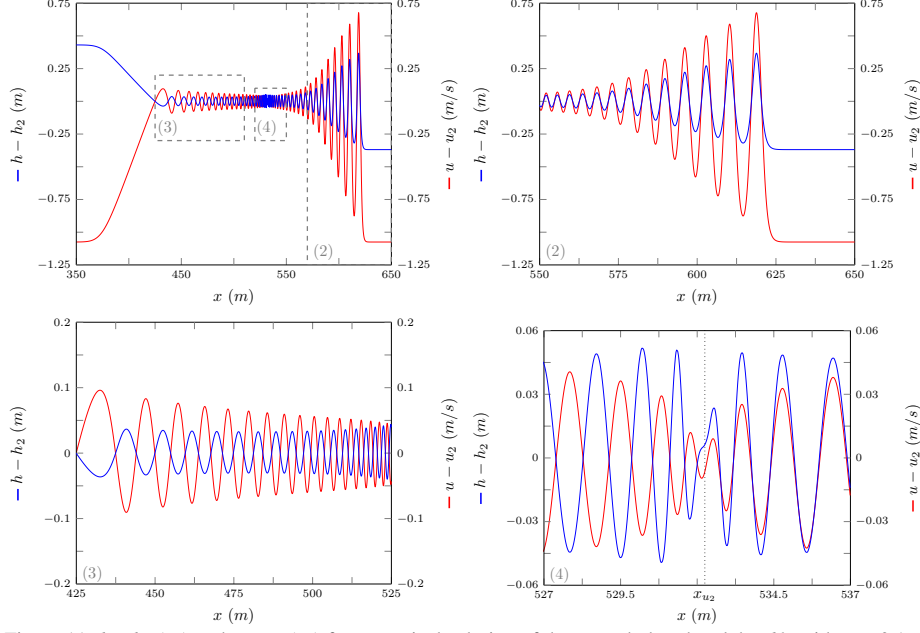


Figure 11:  $h - h_2$  (blue) and  $u - u_2$  (red) for numerical solution of the smooth dam-break by  $\mathcal{V}_3$  with  $\alpha = 0.1m$  and  $\Delta x = 10/2^9 m$  at  $t = 30s$  as in Figure 7.

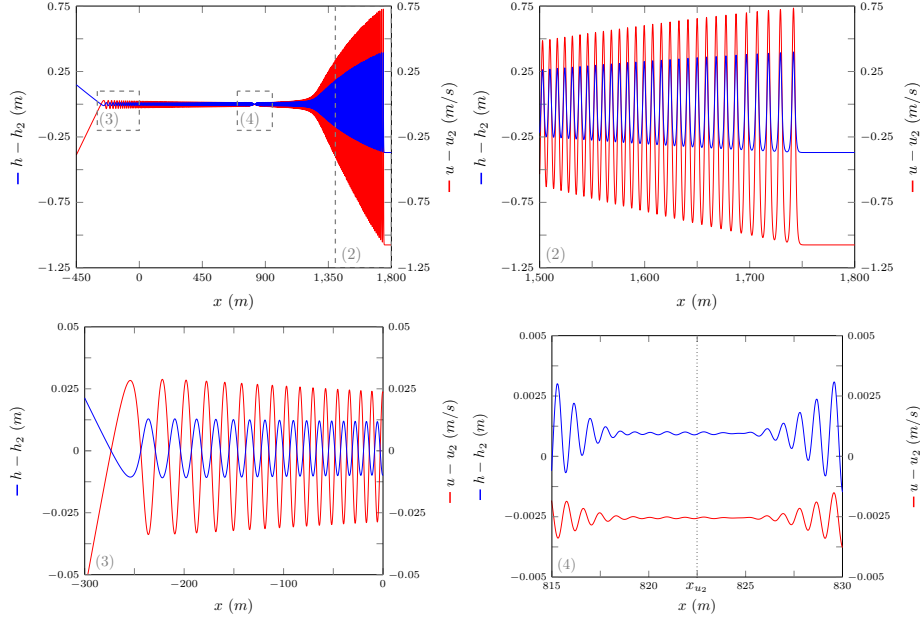


Figure 12:  $h - h_2$  (blue) and  $u - u_2$  (red) for numerical solution of the smooth dam-break by  $\mathcal{V}_3$  with  $\alpha = 0.1m$  and  $\Delta x = 10/2^9 m$  at  $t = 300s$  as in Figure 9.

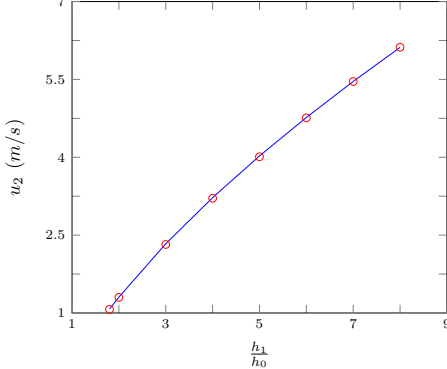


Figure 13:  $u_2$  (—) and speed of the contact discontinuity (○) for numerical solutions of smoothed dam-break problems with different aspect ratios ( $h_1/h_0$ ) by  $\mathcal{V}_3$  where  $\alpha = 0.1\text{m}$  and  $\Delta x = 10/2^9\text{m}$  at  $t = 100\text{s}$ .

in-phase this corresponds to the positive branch  $u + \sqrt{gh} \sqrt{3/(h^2k^2 + 3)}$ . So that the contact discontinuity is the location of the highest wave numbers and it travels at speed  $u$  which would be the mean velocity inside the bore. This explains why the behaviour around the contact discontinuity is sensitive to smoothing of the initial conditions and diffusivity of the method.

A range of different mean bore speeds were modelled with smoothed dam-break problems by fixing  $h_0 = 1\text{m}$  and varying  $h_1$  to allow for different aspect ratios and thus different bore speeds. The results are plotted in Figure 13 which shows that the contact discontinuity travels at a speed close to  $u_2$  for a range of mean bore speeds.

These results demonstrate that while  $h_2$  and  $u_2$  are not exactly the mean behaviour of the bore for the Serre equations the two are highly correlated across a range of different smoothed dam-break problems and so the analytic solutions of the shallow water wave equations are a good guide for the mean behaviour of the Serre equations.

#### 5.4. Whitham modulation comparison

The expressions for the leading wave amplitude  $A^+$  and speed  $S^+$  obtained by [1] are asymptotic results and so we are interested in how our numerical results behave over time. Thus for the dam-break problem in Figure 9 the peak amplitude in region IV (A) was plotted over time in Figure 14. It can be seen that  $A$  approaches a value larger than  $A^+$  over time. We find that as  $\alpha \rightarrow 0$  and  $\Delta x \rightarrow 0$   $A$  converges away from  $A^+$  in this time scale for this aspect ratio. Thus it appears that the true solution of the dam-break for the Serre equations has an amplitude in region IV slightly above  $A^+$ . This is not inconsistent with the results of [1] as their scale comparing  $A^+$  to  $A$  is too large to see such a small difference. From Figure 9 it can be seen that while  $S^+$  does not precisely predict the bore speed it is a better prediction than  $S_2$ .

These results together with those of El et al. [1] demonstrate that  $A$  and  $A^+$  are highly correlated across a range of different smoothed dam-break problems, but for a given problem these two are not precisely equal for our numerical results.

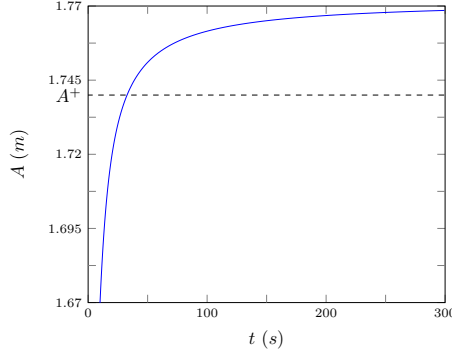


Figure 14: Leading wave height plotted over time for the numerical solution of the smooth dam-break problem by  $\mathcal{V}_3$  with  $\alpha = 0.1m$  for  $\Delta x = 10/2^9 m$  (blue) as in Figure 9.

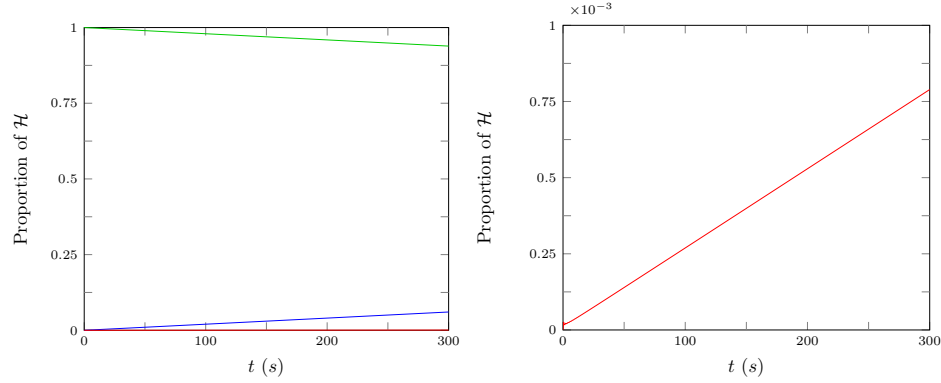


Figure 15: Proportion of  $\mathcal{H}$  made up by horizontal kinetic energy (blue), vertical kinetic energy (red) and gravitational potential energy (green) for  $\mathcal{V}_3$ 's solution of the smooth dam-break problem with  $\alpha = 0.1m$  and  $\Delta x = 10/2^9 m$  over time as in Figure 9.

### 351 5.5. Energy Breakdown

352 The Hamiltonian (2) has 3 terms representing in order, horizontal kinetic energy  
 353  $hu^2$ , vertical kinetic energy  $\frac{h^3}{3} \frac{\partial u}{\partial x}$  and gravitational potential energy  $gh^2$ . It might be  
 354 expected that the oscillations of the undular bore such as in Figure 9 would result in  
 355 significant vertical energies. However, Figure 15 demonstrates that this is not the case,  
 356 as the total vertical kinetic energy in the system is insignificant relative to the other  
 357 energies. This plot also demonstrates that even with dispersive terms and large oscil-  
 358 lations the drivers of change in the dam-break problem are the transfer of gravitational  
 359 potential energy into horizontal kinetic energy which occurs slowly.

### 360 6. Conclusions

361 Utilising two finite difference methods of second-order and three finite difference-  
 362 volume hybrid methods of various orders an investigation into the smoothed dam-break  
 363 problem with varying steepness was performed. Four different behaviours were uncov-  
 364 ered with the general trend being that an increase in steepness increases the size and

365 number of oscillations in the solution. This study explains the different numericals re-  
 366 sults in literature involving the solution of the Serre equations applied to the smoothed  
 367 dam-break problem and also uncovers a new result. We find that while the analytic so-  
 368 lution of the shallow water wave equations for the dam-break problem is a good guide  
 369 to the mean behaviour of the Serre equations the speed and height of the bores do not  
 370 match up precisely. While the Whitham modulation results for the Serre equations give  
 371 better predictions than the shallow water wave equations analytic solution it was found  
 372 that they also do not line up with our numerical results precisely. It was demonstrated  
 373 that the contact discontinuity corresponds to high wave numbers and thus travels at  
 374 the mean velocity inside the bore. Lastly it was shown that vertical kinetic energy is  
 375 negligible for the Serre equations applied to the dam-break problem.

- 376 [1] G. El, R. H. J. Grimshaw, N. F. Smyth, Unsteady undular bores in fully nonlinear  
 377 shallow-water theory, *Physics of Fluids* 18 (027104).
- 378 [2] O. Le Métayer, S. Gavrilyuk, S. Hank, A numerical scheme for the GreenNaghdi  
 379 model, *Journal of Computational Physics* 229 (6) (2010) 2034–2045.
- 380 [3] D. Mitsotakis, B. Ilan, D. Dutykh, On the Galerkin/Finite-Element Method for  
 381 the Serre Equations, *Journal of Scientific Computing* 61 (1) (2014) 166–195.
- 382 [4] D. Mitsotakis, D. Dutykh, J. Carter, On the nonlinear dynamics of the traveling-  
 383 wave solutions of the Serre system, *Wave Motion* 70 (1) (2017) 166–182.
- 384 [5] C. Zoppou, J. Pitt, S. Roberts, Numerical Solution of the Fully Non-linear Weakly  
 385 Dispersive Serre Equations for Steep Gradient Flows, *Applied Mathematical*  
 386 *Modelling* 00 (00) (2017) 00–00.
- 387 [6] C. H. Su, C. S. Gardner, Korteweg-de Vries equation and generalisations. III.  
 388 Derivation of the Korteweg-de Vries equation and Burgers equation, *Journal of*  
 389 *Mathematical Physics* 10 (3) (1969) 536–539.
- 390 [7] D. Lannes, P. Bonneton, Derivation of asymptotic two-dimensional time-  
 391 dependent equations for surface water wave propagation, *Physics of Fluids* 21 (1)  
 392 (2009) 16601–16610.
- 393 [8] M. Li, P. Guyenne, F. Li, L. Xu, High order well-balanced CDG-FE methods  
 394 for shallow water waves by a Green-Naghdi model, *Journal of Computational*  
 395 *Physics* 257 (2014) 169–192.
- 396 [9] Y. A. Li, Hamiltonian Structure and Linear Stability of Solitary Waves of the  
 397 Green-Naghdi Equations, *Journal of Nonlinear Mathematical Physics* 9 (2002)  
 398 99–105.
- 399 [10] A. E. Green, P. M. Naghdi, A derivation of equations for wave propagation in  
 400 water of variable depth, *Journal of Fluid Mechanics* 78 (2) (1976) 237–246.
- 401 [11] C. Wu, G. Huang, Y. Zheng, Theoretical solution of dam-break shock wave, *Jour-*  
 402 *nal of Hydraulic Engineering* 125 (11) (1999) 1210–1215.

- 403 [12] A. A. Harten, High resolution schemes for hyperbolic conservation laws, *Journal*  
404 *of Computational Physics* 49 (3) (1983) 357–393.
- 405 [13] G. El, M. Hoefer, Dispersive shock waves and modulation theory, *Physica D:*  
406 *Nonlinear Phenomena* 333 (2016) 11–65.